

Diffusion Sampling Correction via Approximately 10 Parameters

Guangyi Wang¹, Wei Peng², Lijiang Li¹, Wenyu Chen³, Yuren Cai¹, Songzhi Su^{1*}

¹School of Informatics, Xiamen University

²Department of Psychiatry and Behavioral Sciences, Stanford University

³School of Cyber Science and Technology, Shandong University

wanguangyi@stu.xmu.edu.cn, ssz@xmu.edu.cn

Abstract

Diffusion Probabilistic Models (DPMs) have demonstrated exceptional performance in generative tasks, but this comes at the expense of sampling efficiency. To enhance sampling speed without sacrificing quality, various distillation-based accelerated sampling algorithms have been recently proposed. However, they typically require significant additional training costs and model parameter storage, which limit their practical application. In this work, we propose **PCA-based Adaptive Search (PAS)**, which optimizes existing solvers for DPMs with minimal learnable parameters and training costs. Specifically, we first employ PCA to obtain a few orthogonal unit basis vectors to span the high-dimensional sampling space, which enables us to learn just a set of coordinates to correct the sampling direction; furthermore, based on the observation that the cumulative truncation error exhibits an “S”-shape, we design an adaptive search strategy that further enhances the sampling efficiency and reduces the number of stored parameters to approximately 10. Extensive experiments demonstrate that PAS can significantly enhance existing fast solvers in a plug-and-play manner with negligible costs. For instance, on CIFAR10, PAS requires only **12 parameters and less than 1 minute** of training on a single NVIDIA A100 GPU to optimize the DDIM from 15.69 FID (NFE=10) to 4.37.

1. Introduction

Diffusion Probabilistic Models (DPMs) [10, 13, 35, 39, 40] have demonstrated impressive generative capabilities in various fields, including image generation [7, 29], text-to-image generation [3, 31], video generation [5], and speech synthesis [37], garnering widespread attention. DPMs introduce noise into the data through a forward process and then generate the actual output by iterative denoising during the reverse process. Compared to other generative mod-

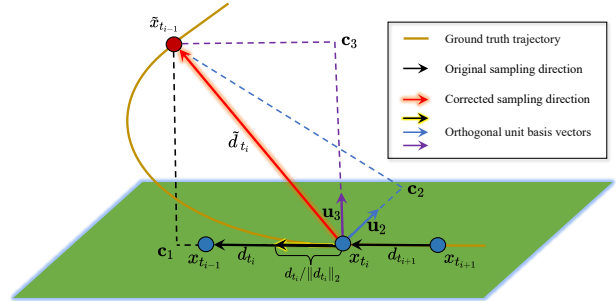


Figure 1. PCA-based sampling correction. We first utilize PCA to obtain a few orthogonal unit vectors that span the space of the sampling trajectories and then learn the coordinates to correct the sampling directions in regions of large curvature along the ground truth trajectory.

els such as Generative Adversarial Networks (GANs) [8] and Variational Autoencoders (VAEs) [16], DPMs offer advantages in generating high-quality outputs and maintaining training stability. However, the denoising process in DPMs often requires hundreds or thousands of iterative steps, resulting in slow sampling speeds that severely hinder practical applications.

Existing sampling algorithms for accelerated DPMs can be categorized into two main categories: training-free and training-based methods. Training-free methods [2, 13, 21, 23, 24, 36, 47, 49, 50] typically reduce discretization errors in each sampling iteration by designing fast solvers through analytical approaches, can achieve sampling quality comparable to the original 1000 number of function evaluations (NFE) with only 20 NFE. However, when NFE is less than 10, the accumulated truncation errors in these methods can be significantly magnified, leading to non-convergent sampling, which is ineffective and remains time-consuming. Training-based methods [22, 32, 41, 44] generally enhance sampling efficiency significantly, with the potential to achieve one-step sampling that matches the quality of the original 1000 NFE. Nonetheless, these meth-

*Corresponding Author.

ods often incur high computational costs and save additional model parameters. Even for the relatively simple CIFAR10 dataset, they may require over 100 A100 GPU hours [32, 41], posing challenges for practical applications. Moreover, training-based methods often establish new paths between noise and data distributions, disrupting the interpolation capability between two disconnected modes.

To address these issues, we propose PCA-based Adaptive Search (PAS), a method that can correct the truncation errors of existing fast solvers with minimal training costs and learnable parameters in a plug-and-play manner. Additionally, PAS retains the interpolation capability between two disconnected modes. Inspired by previous observation that the sampling trajectories of DPMs lie in a low-dimensional subspace embedded in high-dimensional space [51], we propose employing Principal Component Analysis (PCA) to obtain a few orthogonal unit basis vectors in the high-dimensional space of the sampling trajectories, then learning the corresponding coefficients (i.e., coordinates) along each basis vector to determine the correct sampling direction. This approach *avoids training neural networks to directly produce high-dimensional outputs*, significantly reducing the number of learnable parameters and training costs. Furthermore, we observe that the accumulated truncation errors of existing fast solvers exhibit an “S”-shape. We have designed an adaptive search strategy to balance the sampling steps that require correction and the truncation error. This further enhances the sampling efficiency of our method while reducing the amount of parameters required for storage. We validate the effectiveness of PAS on various unconditional and conditional pre-trained DPMs, across five datasets with resolutions ranging from 32 to 512. Results demonstrate that our method can significantly improve the image quality with negligible costs. Our contributions are summarized as follows:

- We propose a new plug-and-play training paradigm with about 10 parameters for existing fast DPMs solvers as an efficient alternative to the high-cost training-based algorithms, rendering the learnable parameters and training costs negligible.
- We design an adaptive search strategy to reduce correction steps, further enhancing the sampling efficiency of our method and decreasing the stored parameters.
- Extensive experiments across various datasets validate the effectiveness of the proposed PAS method in further enhancing the sampling efficiency of existing fast solvers.

2. Background

2.1. Forward and reverse processes

The goal of diffusion probability models (DPMs) [10, 13, 35, 39, 40] is to generate D -dimensional random variables $x_0 \in \mathbb{R}^D$ that follow the data distribution $q_{data}(x_0)$.

DPMs add noise to the data distribution through a forward diffusion process; given x_0 , the latent variables $\{x_t \in \mathbb{R}^D\}_{t \in [0, T]}$ are defined as:

$$q(x_t | x_0) = \mathcal{N}(x_t | \alpha_t x_0, \sigma_t^2 \mathbf{I}), \quad (1)$$

where $\alpha_t \in \mathbb{R}$ and $\sigma_t \in \mathbb{R}$ are scalar functions related to the time step t . Furthermore, Song *et al.* [40] introduced stochastic differential equations (SDE) to model the forward diffusion process, described as:

$$dx_t = f(t)x_t dt + g(t)dw_t, \quad (2)$$

where $f(\cdot) : \mathbb{R} \rightarrow \mathbb{R}$, $g(\cdot) : \mathbb{R} \rightarrow \mathbb{R}$, and $w_t \in \mathbb{R}^D$ is the standard Wiener process [27]. Put together Eq. (1) and Eq. (2), we can get $f(t) = \frac{d \log \alpha_t}{dt}$ and $g^2(t) = \frac{d \sigma_t^2}{dt} - 2 \frac{d \log \alpha_t}{dt} \sigma_t^2$. Additionally, Song *et al.* [40] provided the corresponding reverse diffusion process from time step T to 0 as follows:

$$dx_t = [f(t)x_t - g^2(t)\nabla_x \log q_t(x_t)] dt + g(t)d\bar{w}_t, \quad (3)$$

where $\nabla_x \log q_t(x_t)$ is referred to as the *score function*, which can be estimated through neural networks. Remarkably, Song *et al.* [40] proposed a *probability flow ordinary differential equation* (PF-ODE) with the same marginal distribution as Eq. (3) at any time t , based on the Fokker-Planck equation [28]. Its expression is as follows:

$$dx_t = \left[f(t)x_t - \frac{1}{2}g^2(t)\nabla_x \log q_t(x_t) \right] dt. \quad (4)$$

Unlike Eq. (3), this PF-ODE does not introduce noise into the sampling process, making it a deterministic sampling procedure. Due to its simpler form and more efficient sampling, it is preferred in practical applications over SDE [23, 36, 40].

2.2. Score matching

To solve the PF-ODE in Eq. (4), it is typically necessary to first employ a neural network $s_\theta(x_t, t)$ to estimate the unknown score function $\nabla_x \log q_t(x_t)$ [39, 40]. The neural network s_θ is trained using the L_2 loss as follows:

$$\mathbb{E}_{x_0 \sim q_{data}} \mathbb{E}_{x_t \sim q(x_t | x_0)} \|s_\theta(x_t, t) - \nabla_x \log q_t(x_t)\|_2^2. \quad (5)$$

Additionally, Ho *et al.* [10] proposed using a noise prediction network $\epsilon_\theta(x_t, t)$ to predict the noise added to x_t at time step t . Other literature [13, 24] suggested using a data prediction network $x_\theta(x_t, t)$ to directly predict x_0 at different time steps t . The relationship among these three prediction networks can be expressed as follows:

$$s_\theta(x_t, t) = -\frac{\epsilon_\theta(x_t, t)}{\sigma_t} = \frac{x_\theta(x_t, t) - x_t}{\sigma_t^2}. \quad (6)$$

In this paper, we adopt the settings from EDM [13], specifically $f(t) = 0$, $g(t) = \sqrt{2t}$, derived from Eqs. (2) to (4), and $\alpha_t = 1$, $\sigma_t = t$ as stated in Eq. (1). Furthermore, utilizing the noise prediction network ϵ_θ , Eq. (4) can be expressed as:

$$dx_t = \epsilon_\theta(x_t, t)dt. \quad (7)$$

According to the simple PF-ODE form in Eq. (7), using the Euler-Maruyama (Euler) solver [17], the sampling process from t_i to t_{i-1} can be represented as:

$$x_{t_{i-1}} \approx x_{t_i} + (t_{i-1} - t_i)\epsilon_\theta(x_{t_i}, t_i), \quad (8)$$

where $i \in [N, \dots, 1]$ and $t_N = T, \dots, t_0 = 0$.

3. The proposed PAS method

3.1. PCA-based sampling correction

Utilizing the Euler solver [17] with Eq. (8) to approximate Eq. (7) introduces notable discretization errors that can become significantly amplified with a limited number of iterations. The exact solution of Eq. (7) is given by:

$$x_{t_{i-1}} = x_{t_i} + \int_{t_i}^{t_{i-1}} \epsilon_\theta(x_t, t)dt. \quad (9)$$

Let sampling direction $d_{t_i} := \epsilon_\theta(x_{t_i}, t_i)$. Existing fast solvers reduce discretization errors through various numerical approximations. For example, the PNDM [21] employs linear multi-step methods, while the DPM-Solver [23, 24] utilizes Taylor expansion to correct the sampling direction d_{t_i} in Eq. (8) to approach the exact solution $\int_{t_i}^{t_{i-1}} \epsilon_\theta(x_t, t)dt$. Training-based methods [32, 41, 51] typically utilize neural networks to correct the direction d_{t_i} . In contrast to the aforementioned methods, we extract a few orthogonal unit basis vectors from the high-dimensional space of the sampling trajectory using PCA. By learning the coordinates corresponding to these basis vectors, we correct the direction d_{t_i} to the optimal direction \tilde{d}_{t_i} , thereby minimizing the training cost.

Specifically, during the iteration process from x_{t_i} to $x_{t_{i-1}}$, we first extract a set of basis vectors from the space of the existing sampling trajectories $\{x_{t_N}, \dots, x_{t_i}\}$, where $t_N = T, \dots, t_0 = 0$. A surprising finding is that when performing PCA to decompose the entire sampling trajectory $\{x_{t_i}\}_{i=N}^0$, the cumulative percent variance saturates rapidly; by the time the number of principal components reaches 3, the cumulative percent variance approaches nearly 100%. This indicates that the entire sampling trajectory lies in a three-dimensional subspace embedded in a high-dimensional space, the finding initially revealed in work [51]. Furthermore, according to Eq. (8), $x_{t_{i-1}}$ is a linear combination of x_{t_i} and d_{t_i} , allowing us to modify the existing trajectory $\{x_{t_N}, \dots, x_{t_i}\}$ to $\{x_{t_N}, d_{t_N}, \dots, d_{t_{i+1}}\}$. This modification enables our

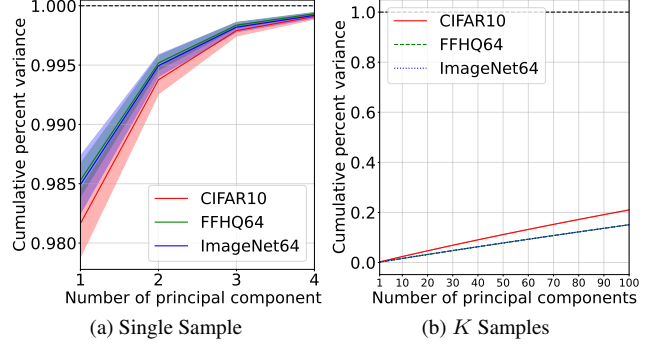


Figure 2. We utilize PCA to analyze the sampling trajectories, illustrating the trend of cumulative percent variance as the number of principal components varies. The trajectories are obtained from 1k samples using the Euler solver [17] in the EDM [13] pre-trained model with 100 NFE. (a) The average results of each trajectory $\{x_T, \{d_{t_i}\}_{i=N}^1\}$. (b) The results of K trajectories $\{\{x_{t_i}^k\}_{i=N}^0\}_{k=1}^K$ (FFHQ and ImageNet curves nearly overlap).

method to share buffers during the sampling process when combined with existing multi-step solvers that utilize historical gradients (*e.g.*, PNDM [21], DEIS [47], etc.) to optimize memory usage. To validate the reasonableness of this modification, we perform PCA on a complete sampling trajectory $\{x_T, \{d_{t_i}\}_{i=N}^1\}$, with the resulting cumulative percent variance illustrated in Fig. 2a, showing that *three principal components suffice to span the space occupied by the entire sampling trajectory*. Notably, the sampling trajectories of different samples do not lie in the same three-dimensional subspace. We apply PCA to decompose the set of K sampling trajectories from K samples $\{\{x_{t_i}^k\}_{i=N}^0\}_{k=1}^K$, with the resulting cumulative percent variance displayed in Fig. 2b. We observe that the cumulative percent variance does not show a saturation trend as the number of principal components increases.

Based on this, during the iterative process from x_{t_i} to $x_{t_{i-1}}$, we decompose the existing sampling trajectory, requiring only the top three basis vectors to span the space of the sampling trajectory. Let $\mathbf{X} = \{x_{t_N}, d_{t_N}, \dots, d_{t_{i+1}}\}$, where $\mathbf{X} \in \mathbb{R}^{(N-i+1) \times D}$ and D denotes the dimension of x_{t_N} . When using the top k principal components, the process is described as:

$$\mathbf{W}\Sigma\mathbf{V}^T = \text{SVD}(\mathbf{X}), \quad (10)$$

$$\{\mathbf{v}_j\}_{j=1}^k = \mathbf{V}[:, :k], \quad (11)$$

where SVD denotes the Singular Value Decomposition (SVD) and $\mathbf{v}_j \in \mathbb{R}^{D \times 1}$ represent orthogonal unit basis vectors. Further, since our goal is to correct the current direction d_{t_i} , we modify the above PCA process by directly specifying $\mathbf{v}_1 = d_{t_i} / \|d_{t_i}\|_2$. The subsequent approach generally involves computing the projection of \mathbf{X} onto the basis

vector \mathbf{v}_1 , as follows:

$$\text{proj}_{\mathbf{v}_1}(\mathbf{X}) = \frac{\mathbf{X}\mathbf{v}_1}{\|\mathbf{v}_1\|_2^2}\mathbf{v}_1^T. \quad (12)$$

Then apply PCA to decompose $\mathbf{X} - \text{proj}_{\mathbf{v}_1}(\mathbf{X})$, obtaining the remaining two orthogonal unit basis vectors.

To further optimize computation time, we omit the projection step. After specifying $\mathbf{v}_1 = d_{t_i}/\|d_{t_i}\|_2$, we modify \mathbf{X} as follows:

$$\mathbf{X}' = \text{Concat}(\mathbf{X}, d_{t_i}), \quad (13)$$

where $\mathbf{X}' \in \mathbb{R}^{(N-i+2) \times D}$. Subsequently, we decompose \mathbf{X}' using Eq. (10) to obtain \mathbf{V}' , and then extract two new basis vectors, $\mathbf{v}'_1, \mathbf{v}'_2 = \mathbf{V}'[:, :2]$. Due to the omission of the projection step, the new basis vectors may be collinear with \mathbf{v}_1 . Nevertheless, we only need to add one new basis vector $\mathbf{v}'_3 = \mathbf{V}'[:, 2]$, sufficient to ensure that the sampling trajectory lies within the span of the basis vectors. Through Schmidt orthogonalization, we can obtain new orthogonal unit basis vectors as follows:

$$\mathbf{U} = [\mathbf{u}_1, \mathbf{u}_2, \mathbf{u}_3, \mathbf{u}_4] = \text{Schmidt}(\mathbf{v}_1, \mathbf{v}'_1, \mathbf{v}'_2, \mathbf{v}'_3), \quad (14)$$

where Schmidt represents the Schmidt orthogonalization and $\mathbf{U} \in \mathbb{R}^{D \times 4}$ consists of four orthogonal unit basis vectors. It is noteworthy that increasing a basis vector incurs less computational cost relative to the projection operation, and the additional single parameter can be considered negligible. After obtaining the basis vectors \mathbf{U} that span the space of the sampling trajectory, we can initialize the learnable coordinate parameters. Since our goal is to correct the sampling direction d_{t_i} , and we have already specified the first basis vector $\mathbf{u}_1 = \mathbf{v}_1 = d_{t_i}/\|d_{t_i}\|_2$, we initialize the first coordinate as $\mathbf{c}_1 = \|d_{t_i}\|_2$, with the remaining coordinates initialized to zero, as follows:

$$\mathbf{C} = [\mathbf{c}_1 = \|d_{t_i}\|_2, \mathbf{c}_2 = 0, \mathbf{c}_3 = 0, \mathbf{c}_4 = 0]. \quad (15)$$

At this point, we have $d_{t_i} = \mathbf{U}\mathbf{C}^T$. Through training, we can obtain the optimized $\tilde{\mathbf{C}}$, thereby acquiring the corrected direction $\tilde{d}_{t_i} = \mathbf{U}\tilde{\mathbf{C}}^T$. The specific PCA-based sampling correction schematic is illustrated in Fig. 1. In summary, we employ PCA to correct the sampling direction, requiring only a few sets of coordinates as learnable parameters. This approach serves as an efficient alternative to high-cost training-based algorithms, leveraging the geometric characteristics of the sampling trajectory in a low-dimensional space. As a result, it significantly reduces the number of learnable parameters and training costs.

3.2. Training and sampling

To correct the update direction d_{t_i} during the iterative process from x_{t_i} to $x_{t_{i-1}}$, we need to learn the coordinates \mathbf{C} in

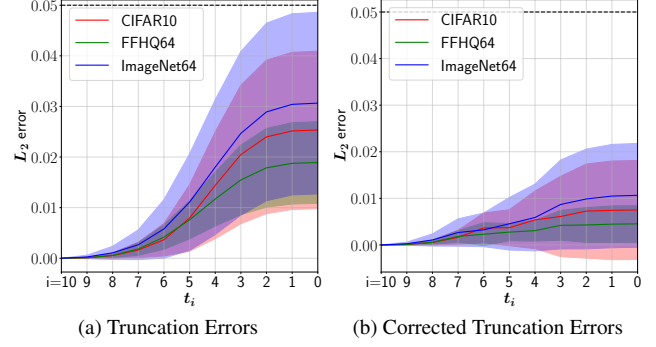


Figure 3. The truncation errors are evaluated using the Euler solver [17] both with and without the proposed PAS. We utilize the EDM [13] pre-trained model to sample 10k samples and compute the average L_2 distance of 10 NFE compared to the ground truth trajectory (100 NFE). (a) The “S”-shaped truncation error is produced by the Euler solver. (b) The truncation error is corrected using PAS. Notably, PAS adaptively corrects only the parts of the sampling trajectory with large curvature.

Eq. (15) to apply to the sampling trajectory of all samples. First, given any first-order ODE solver ϕ , the discretized solution of Eq. (9) can be uniformly represented as follows:

$$x_{t_{i-1}} = \phi(x_{t_i}, d_{t_i}, t_i, t_{i-1}), \quad (16)$$

where $d_{t_i} = \mathbf{U}\mathbf{C}^T = \epsilon_\theta(x_{t_i}, t_i)$. Given the ground truth $x_{t_{i-1}}^{gt}$, we can train the coordinates \mathbf{C} using the stochastic gradient descent (SGD) algorithm [30], with the L_2 loss update process as follows:

$$\tilde{\mathbf{C}} \leftarrow \mathbf{C} - \alpha \nabla_{\mathbf{C}} \|x_{t_{i-1}} - x_{t_{i-1}}^{gt}\|_2^2, \quad (17)$$

where α denotes the learning rate, and the specific acquisition method for $x_{t_{i-1}}^{gt}$ is discussed in Sec. 3.3. After training \mathbf{C} using multiple samples through Eq. (17), we obtain the trained coordinates $\tilde{\mathbf{C}}$.

During the iterative process from x_{t_i} to $x_{t_{i-1}}$, by utilizing the trained coordinates $\tilde{\mathbf{C}}$, we can correct the current update direction d_{t_i} to $\tilde{d}_{t_i} = \mathbf{U}\tilde{\mathbf{C}}^T$, thereby obtaining a more accurate $\tilde{x}_{t_{i-1}}$, as follows:

$$\tilde{x}_{t_{i-1}} = \phi(x_{t_i}, \tilde{d}_{t_i}, t_i, t_{i-1}). \quad (18)$$

3.3. Adaptive search

In Secs. 3.1 and 3.2, we introduced how to correct the iterative process from x_{t_i} to $x_{t_{i-1}}$ using our method. This section describes how to correct the iterative process from x_T to x_0 using our approach. First, we need to generate a ground truth trajectory $\{x_{t_i}^{gt}\}_{i=N}^0$ to correct $\{x_{t_i}\}_{i=N}^0$, where $x_{t_N}^{gt} = x_{t_N}$. In this paper, we adopt a widely used polynomial time schedule [13] for both sampling and generating the ground truth trajectory, which is expressed as

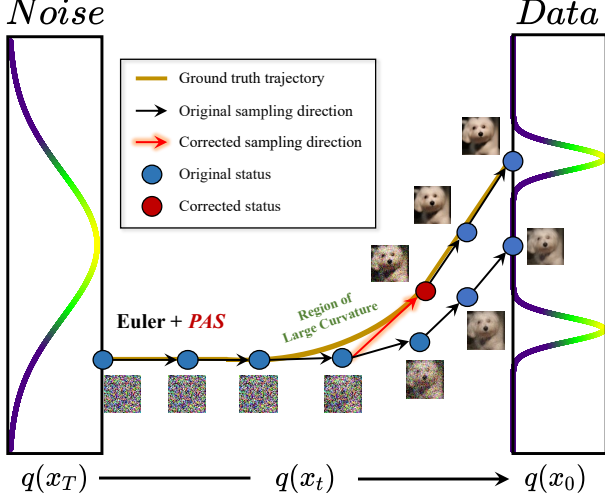


Figure 4. Illustration of PCA-based Adaptive Search (PAS). We demonstrate the Euler solver [17] with the proposed PAS method, where sampling directions are derived from the tangent direction of the ground truth trajectory. The details of the correction process for the sampling direction are presented in Fig. 1.

follows:

$$t_i = (t_0^{1/\rho} + \frac{i}{N}(t_N^{1/\rho} - t_0^{1/\rho}))^\rho, i \in [N, \dots, 0], \quad (19)$$

where $t_N = T, \dots, t_0 = \epsilon$, and ϵ is a value approaching zero. To obtain the ground truth trajectory, we simply need to insert more sampling steps into the time schedule from Eq. (19) to achieve a more accurate solution. Specifically, consider using a teacher Euler solver with N' NFE to guide a student Euler solver with $N (< N')$ NFE during training. First, we insert M values into the time schedule for the student solver, such that M is the smallest positive integer satisfying $N(M+1) \geq N'$. Next, we use Eq. (19) to generate the time schedule for the teacher solver: $t_{N(M+1)} = T, \dots, t_0 = \epsilon$. Finally, we only need to index the $x_{t_{i(M+1)}}$ from the teacher solver using the $i \in [N, \dots, 0]$, thereby obtaining the ground truth trajectory $\{x_{t_i}^{gt}\}_{i=N}^0 = \{x_{t_{i(M+1)}}\}_{i=N}^0$.

After obtaining the ground truth trajectory $\{x_{t_i}^{gt}\}_{i=N}^0$, we need to sequentially correct d_{t_N}, \dots, d_{t_1} . This is because once d_{t_N} is corrected to \tilde{d}_{t_N} , $x_{t_{N-1}}$ will be adjusted accordingly to $\tilde{x}_{t_{N-1}}$. This further modifies the next time point direction that requires correction: $d_{t_{N-1}} = \epsilon_\theta(\tilde{x}_{t_{N-1}}, t_{N-1})$. In general, we need to correct N directions sequentially, storing $4N$ learned coordinate parameters, and correcting N iterative processes during sampling. Nevertheless, to further reduce the additional computational cost during the sampling process and the number of stored coordinate parameters, we propose an adaptive search strategy. Specifically, the cumulative truncation error of the existing solvers exhibits an “S”-shaped trend, as shown in Fig. 3a, indicat-

Algorithm 1 PCA-based Adaptive Search (PAS)

Require: initial value x_T , NFE N , model ϵ_θ , given solver ϕ , time steps $\{t_i\}_{i=N}^0$, a ground truth trajectory $\{x_{t_i}^{gt}\}_{i=N}^0$, tolerance τ

- 1: **def** PCA(Q, d_{t_i}):
- 2: $\mathbf{W}\Sigma\mathbf{V}^T = \text{SVD}(\text{Concat}(Q, d_{t_i}))$
- 3: $\mathbf{v}_1 = d_{t_i}/\|d_{t_i}\|_2; \mathbf{v}'_1, \mathbf{v}'_2, \mathbf{v}'_3 = \mathbf{V}[:, :3]$
- 4: $\mathbf{u}_1, \mathbf{u}_2, \mathbf{u}_3, \mathbf{u}_4 = \text{Schmidt}(\mathbf{v}_1, \mathbf{v}'_1, \mathbf{v}'_2, \mathbf{v}'_3)$
- 5: **return** $[\mathbf{u}_1, \mathbf{u}_2, \mathbf{u}_3, \mathbf{u}_4]$
- 6: $Q \leftarrow^{\text{buffer}} x_T, d_{t_N} = \epsilon_\theta(x_T, t_N)$
- 7: **for** $i \leftarrow N$ to 1 **do**
- 8: Init $\mathbf{c}_1 = \|d_{t_i}\|_2, \mathbf{c}_2 = 0, \mathbf{c}_3 = 0, \mathbf{c}_4 = 0$
- 9: $\mathbf{C} = [\mathbf{c}_1, \mathbf{c}_2, \mathbf{c}_3, \mathbf{c}_4], \mathbf{U} = \text{PCA}(Q, d_{t_i})$
- 10: $x_{t_{i-1}} = \phi(x_{t_i}, \mathbf{U}\mathbf{C}^T, t_i, t_{i-1})$
- 11: $\tilde{\mathbf{C}} \leftarrow \mathbf{C} - \alpha \nabla_{\mathbf{C}} \|x_{t_{i-1}} - x_{t_{i-1}}^{gt}\|_2^2$
- 12: $\tilde{x}_{t_{i-1}} = \phi(x_{t_i}, \mathbf{U}\tilde{\mathbf{C}}^T, t_i, t_{i-1})$
- 13: $\mathcal{L}_1 = \|\tilde{x}_{t_{i-1}} - x_{t_{i-1}}^{gt}\|_2^2, \mathcal{L}_2 = \|x_{t_{i-1}} - x_{t_{i-1}}^{gt}\|_2^2$
- 14: **if** $\mathcal{L}_2 - (\mathcal{L}_1 + \tau) > 0$ **then**
- 15: coordinate_dict[i] = $\tilde{\mathbf{C}}$
- 16: $x_{t_{i-1}} = \tilde{x}_{t_{i-1}}, d_{t_i} = \mathbf{U}\tilde{\mathbf{C}}^T$
- 17: **end if**
- 18: $Q \leftarrow^{\text{buffer}} d_{t_i}, d_{t_{i-1}} = \epsilon_\theta(x_{t_{i-1}}, t_{i-1})$
- 19: **end for**
- 20: **return** coordinate_dict

Algorithm 2 Sampling Correction

Require: initial value x_T , NFE N , model ϵ_θ , given solver ϕ , time steps $\{t_i\}_{i=N}^0$, coordinate_dict

- 1: $Q \leftarrow^{\text{buffer}} x_T, d_{t_N} = \epsilon_\theta(x_T, t_N)$
- 2: **for** $i \leftarrow N$ to 1 **do**
- 3: **if** i in coordinate_dict.key() **then**
- 4: $\mathbf{C} = \text{coordinate_dict}[i], \mathbf{U} = \text{PCA}(Q, d_{t_i})$
- 5: $d_{t_i} = \mathbf{U}\mathbf{C}^T$
- 6: **end if**
- 7: $x_{t_{i-1}} = \phi(x_{t_i}, d_{t_i}, t_i, t_{i-1})$
- 8: $Q \leftarrow^{\text{buffer}} d_{t_i}, d_{t_{i-1}} = \epsilon_\theta(x_{t_{i-1}}, t_{i-1})$
- 9: **end for**
- 10: **return** x_{t_0}

ing that it initially grows slowly, then increases rapidly, and ultimately returns to a slow growth rate. Thus, we can infer that the sampling trajectory first appears linear, then transitions to a curve, and ultimately becomes linear again under the attraction of a certain mode. Consequently, *only the parts of the sampling trajectory with large curvature require correction*; the linear sections do not. We employ PCA to obtain the basis of the space containing the sampling trajectory, also aiming to compensate for the missing directions in other bases due to discretization of Eq. (9) in cases of large curvature. The specific implementation of the adap-

tive search is determined by the loss of the optimized state. When using L_2 loss, we obtain:

$$\mathcal{L}_1 = \|\tilde{x}_{t_{i-1}} - x_{t_{i-1}}^{gt}\|_2^2, \mathcal{L}_2 = \|x_{t_{i-1}} - x_{t_{i-1}}^{gt}\|_2^2, \quad (20)$$

where $\tilde{x}_{t_{i-1}}$ is the corrected state. We introduce a tolerance τ to determine whether $\mathcal{L}_2 - (\mathcal{L}_1 + \tau)$ is greater than zero. If it is greater than zero, correction is required for that step; otherwise, the step is considered to lie within the linear part of the sampling trajectory, and no correction is necessary. The tolerance τ is set to a positive value, *e.g.* 10^{-4} . The truncation error after correction using our algorithm is depicted in Fig. 3b, clearly showing a significant reduction in truncation error in the large curvature regions. Now that we have thoroughly presented the proposed PCA-based Adaptive Search (PAS) algorithm, detailing the complete training and sampling processes in Algorithms 1 and 2. The specific schematic is illustrated in Fig. 4.

3.4. Comparing with training-based methods

As discussed in Sec. 1, while training-based methods can achieve one-step sampling [22, 32, 41, 44], they often incur substantial training costs (*e.g.*, exceeding 100 A100 GPU hours on simple CIFAR10). Moreover, these methods tend to disrupt the original ODE trajectories, leading to a loss of interpolation capability between two disconnected modes. Although some low-cost training methods [1, 11, 14, 15, 26, 46, 51] have been proposed, as discussed in Appendix A, these methods still do not address the essential issue and require training a new, relatively small neural network.

In contrast to these methods, PAS introduces a new training paradigm that *corrects high-dimensional vectors by learning low-dimensional coordinates*, achieving minimal learnable parameters and training costs. For instance, using a single NVIDIA A100 GPU, training on CIFAR10 takes only **0~2 minutes**, and merely **10~20 minutes** on datasets with a maximum resolution of 256. Additionally, based on adaptive search, PAS only requires correcting 1~3 time points on the CIFAR10, as shown in Tab. 1 (results for additional datasets, see Tab. 6 in Appendix C.1). This means that PAS only requires **4~12 parameters** during the sampling correction process. This is not in the same order of magnitude as the aforementioned training-based methods. Furthermore, PAS preserves the original ODE trajectories, thereby retaining the interpolation capability of DPMs.

| Method | NFE | | | |
|-------------|-----|-------|-------|-------|
| | 5 | 6 | 8 | 10 |
| DDIM + PAS | 3,1 | 4,2,1 | 5,3,2 | 6,4,2 |
| iPNDM + PAS | 2 | 3 | 3,1 | 4,2 |

Table 1. On the CIFAR10, time points i are corrected by PAS for the DDIM and iPNDM solvers, ranging from NFE (N) to 1.

4. Experiments

To validate the effectiveness of PAS as a plug-and-play and low-cost training method, we conducted extensive experiments on both conditional [13, 31] and unconditional [13, 41] pre-trained models.

4.1. Settings

In this paper, we uniformly adopt the design from the EDM framework [13], as shown in Eq. (7). Regarding the time schedule, we utilize the widely used polynomial schedule with $\rho = 7$, as described in Eq. (19).

Datasets and pre-trained models. We employ PAS across a wide range of image resolutions (from 32 to 512). This includes CIFAR10 32×32 [18], FFHQ 64×64 [12], ImageNet 64×64 [6], LSUN Bedroom 256×256 [45], and images generated by Stable Diffusion v1.4 [31] with 512 resolution. Among these, the CIFAR10, FFHQ, and LSUN Bedroom datasets are derived from the pixel-space unconditional pre-trained models [13, 41]; the ImageNet comes from the pixel-space conditional pre-trained model [13]; and the Stable Diffusion v1.4 [31] belongs to the conditional latent-space pre-trained model.

Solvers. We provide comparative results from previously state-of-the-art fast solvers, including DDIM [36], Heun’s 2nd [13], DPM-Solver-2 [23], DPM-Solver++ [24], DEIS-tAB3 [47], UniPC [49], DPM-Solver-v3 [50], and improved PNDM (iPNDM) [21, 47].

Evaluation. We evaluate the sample quality using the widely adopted Fréchet Inception Distance (FID \downarrow) [9] metric. For Stable Diffusion, we sample 10k samples from the MS-COCO [20] validation set to compute the FID, while for other datasets, we uniformly sample 50k samples.

Training. In Sec. 4.3 and Appendix C.2, we present ablation experiments related to the hyperparameters involved in training, and Appendix B provides detailed training configurations for different datasets that we used. Below, we outline some recommended settings for training hyperparameters: utilizing Heun’s 2nd solver [13] from EDM to generate 5k ground truth trajectories with 100 NFE, employing the L_1 loss function, setting the learning rate to 10^{-2} , and using a tolerance τ of 10^{-4} .

4.2. Main results.

In this section, we present the experimental results of PAS across various datasets and pre-trained models with $NFE \in \{5, 6, 8, 10\}$. In Tab. 2, we report the experimental results of PAS correcting DDIM (equivalent to the Euler solver [17] in the EDM framework [13]) and iPNDM solvers, covering the CIFAR10, FFHQ, ImageNet, and LSUN Bedroom datasets. Notably, for the LSUN Bedroom, the order of iPNDM is set to 2; for the other datasets, the order is set to 3, which yields better average performance (for more results regarding the

| Method | NFE | | | |
|--|--------------|--------------|--------------|-------------|
| | 5 | 6 | 8 | 10 |
| CIFAR10 32×32 [18] | | | | |
| DDIM [36] | 49.68 | 35.63 | 22.32 | 15.69 |
| DDIM + PAS (Ours) | 17.13 | 12.11 | 7.07 | 4.37 |
| Heun’s 2nd [13] | \ | 99.74 | 38.06 | 15.93 |
| DPM-Solver-2 [23] | \ | 60.00 | 10.30 | 5.01 |
| DPM-Solver++(3M) [24] | 31.65 | 17.89 | 8.30 | 5.16 |
| DEIS-tAB3 [47] | 17.65 | 11.84 | 6.82 | 5.64 |
| UniPC(3M) [49] | 31.44 | 17.74 | 8.42 | 5.31 |
| iPNDM [21, 47] | 16.55 | 9.74 | 5.23 | 3.69 |
| iPNDM + PAS (Ours) | 13.61 | 7.47 | 3.87 | 2.84 |
| FFHQ 64×64 [12] | | | | |
| DDIM [36] | 43.92 | 35.21 | 24.38 | 18.37 |
| DDIM + PAS (Ours) | 29.07 | 17.63 | 8.16 | 5.61 |
| Heun’s 2nd [13] | \ | 142.39 | 57.21 | 29.54 |
| DPM-Solver-2 [23] | \ | 83.17 | 22.84 | 9.46 |
| DPM-Solver++(3M) [24] | 23.50 | 14.93 | 9.58 | 6.96 |
| DEIS-tAB3 [47] | 19.47 | 11.61 | 8.64 | 7.07 |
| UniPC(3M) [49] | 22.82 | 14.30 | 10.07 | 7.39 |
| iPNDM [21, 47] | 17.26 | 11.31 | 6.82 | 4.95 |
| iPNDM + PAS (Ours) | 15.89 | 10.29 | 5.85 | 4.28 |
| ImageNet 64×64 [6] | | | | |
| DDIM [36] | 43.81 | 34.03 | 22.59 | 16.72 |
| DDIM + PAS (Ours) | 31.37 | 26.21 | 12.33 | 9.13 |
| Heun’s 2nd [13] | \ | 89.63 | 37.65 | 16.46 |
| DPM-Solver-2 [23] | \ | 44.83 | 12.42 | 6.84 |
| DPM-Solver++(3M) [24] | 27.72 | 17.18 | 8.88 | 6.44 |
| DEIS-tAB3 [47] | 21.06 | 14.16 | 8.43 | 6.36 |
| UniPC(3M) [49] | 27.14 | 17.08 | 9.19 | 6.89 |
| iPNDM [21, 47] | 19.75 | 13.48 | 7.75 | 5.64 |
| iPNDM + PAS (Ours) | 23.33 | 12.89 | 7.27 | 5.32 |
| LSUN Bedroom 256×256 [45] (pixel-space) | | | | |
| DDIM [36] | 34.34 | 25.25 | 15.71 | 11.42 |
| DDIM + PAS (Ours) | 28.22 | 13.31 | 7.26 | 6.23 |
| Heun’s 2nd [13] | \ | 125.46 | 38.64 | 19.12 |
| DPM-Solver-2 [23] | \ | 80.59 | 23.26 | 9.61 |
| DPM-Solver++(3M) [24] | 17.39 | 11.97 | 9.86 | 7.11 |
| DEIS-tAB3 [47] | 16.31 | 11.75 | 7.00 | 5.18 |
| UniPC(3M) [49] | 17.29 | 12.73 | 11.91 | 7.79 |
| iPNDM [21, 47] | 18.15 | 12.90 | 7.98 | 6.17 |
| iPNDM + PAS (Ours) | 15.48 | 10.24 | 6.67 | 5.14 |

Table 2. Sample quality measured by Fréchet Inception Distance (FID \downarrow) on CIFAR10, FFHQ, ImageNet, and LSUN Bedroom datasets. “\” indicates missing data due to the inherent characteristics of the algorithm.

order of iPNDM, see Appendix C.3). The experimental results demonstrate that, regardless of whether dealing with large or small resolution and conditional or unconditional pre-trained models, PAS effectively enhances the sampling

quality of both DDIM and iPNDM solvers. Particularly, PAS combined with iPNDM surpasses the previously state-of-the-art solvers. Notably, PAS significantly optimizes the convergence of the DDIM solver in cases of fewer NFE; for instance, with 10 NFE, PAS achieves FID scores of 4.37, 5.61, 9.13, and 6.23 on the CIFAR10, FFHQ, ImageNet, and LSUN Bedroom datasets, respectively. For Stable Diffusion, we report the experimental results of PAS correcting DDIM. Additionally, we introduce previous state-of-the-art methods, including DPM-Solver++, UniPC, and DPM-Solver-v3, for comparison. These methods utilize their optimal configurations on Stable Diffusion, including the 2M version and logSNR schedule [23], etc. As shown in Tab. 3, PAS significantly improves the sampling quality of DDIM on Stable Diffusion. Notably, the performance of PAS when combined with DDIM surpasses the sampling results of previous state-of-the-art methods, further validating the effectiveness of the proposed PAS.

In Fig. 5 and Appendix C.4, we present the visualization results for Stable Diffusion, as well as for the CIFAR10, FFHQ, ImageNet, and Bedroom datasets. The results indicate that the samples generated by PAS exhibit *higher quality and richer detail*. Through the aforementioned experiments, we have demonstrated that PAS serves as a plug-and-play, low-cost training method that can effectively enhance the performance of existing fast solvers (including DDIM and iPNDM), thereby validating the effectiveness of PAS.

| Method | NFE | | | |
|---------------------------------|--------------|--------------|--------------|--------------|
| | 5 | 6 | 8 | 10 |
| DDIM [36] | 23.42 | 20.08 | 17.72 | 16.56 |
| [†] DPM-Solver++ [24] | 18.87 | 17.44 | 16.40 | 15.93 |
| [†] UniPC [49] | 18.77 | 17.32 | 16.20 | 16.15 |
| [†] DPM-Solver-v3 [50] | 18.83 | 16.41 | 15.41 | 15.32 |
| DDIM + PAS (Ours) | 17.70 | 15.93 | 14.74 | 14.23 |

Table 3. Sample quality measured by FID \downarrow on Stable Diffusion v1.4 with a guidance scale of 7.5. [†]We borrow the results reported in Zheng *et al.* [50] directly.

4.3. Ablation study

In this section, we conduct ablation experiments on several key modules used during the training process, as illustrated in Fig. 6. Additionally, ablation experiments on the learning rate, the solver for generating trajectories, and the tolerance τ are presented in the Appendix C.2. Notably, the selection of these modules in the overall PAS is not a critical factor and only has a slight impact on performance.

Adaptive search. In Fig. 6a, we present the experimental results comparing the PAS with and without the adaptive search strategy (-AS). The findings reveal that the sampling quality of the PAS(-AS) is even inferior to DDIM.

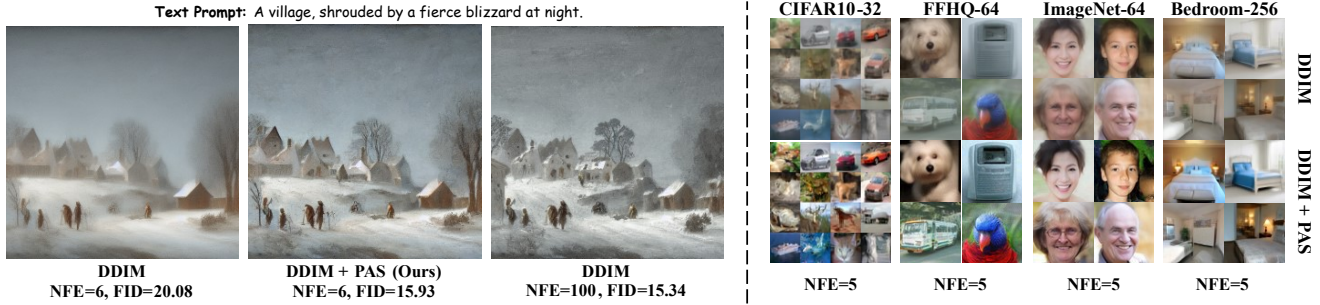


Figure 5. Visualization results using DDIM with and without the proposed PAS. Left: Sampling results on Stable Diffusion v1.4 with a guidance scale of 7.5. Right: Sampling results on the CIFAR10, FFHQ 64×64 , ImageNet 64×64 , and LSUN Bedroom 256×256 datasets.

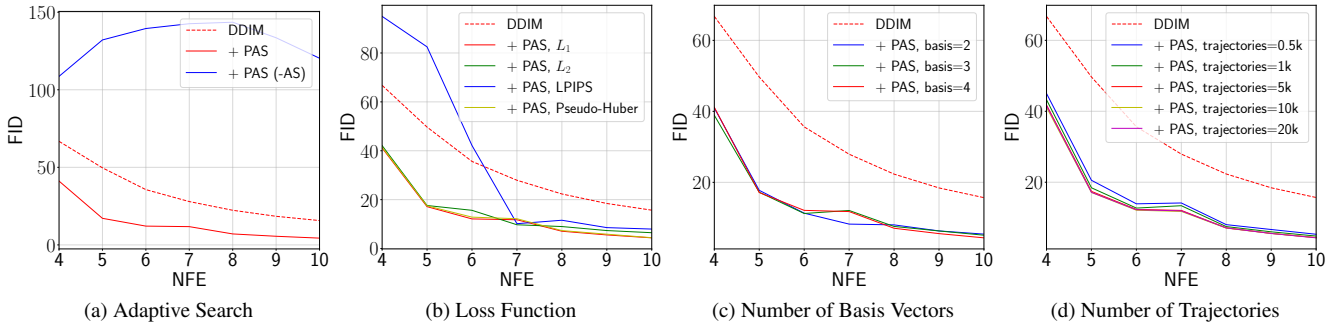


Figure 6. Ablation study on CIFAR10, utilizing PAS to correct DDIM, exploring the impact of adaptive search, loss function, the number of orthogonal unit basis vectors, and the number of ground truth trajectories on FID (recommended setting: the red solid line).

This degradation may be attributed to the linear segments in the sampling trajectory, where the errors from DDIM are negligible. However, the PCA-based sampling correction does not reduce error and instead introduces biases in other basis vectors. This further validates the necessity and effectiveness of the proposed *overall* PAS.

Loss function. We evaluated the L_1 , L_2 , and previously established effective loss functions: LPIPS [48] and Pseudo-Huber [38]. Here, the hyperparameter c for the Pseudo-Huber was set to 0.03, as recommended by Song and Dhariwal [38]. The results are presented in Fig. 6b. Surprisingly, LPIPS exhibits the lowest average performance. Overall, the L_1 loss function demonstrates superior average performance, which may be attributed to its larger scale.

Number of basis vectors. We demonstrate the ablation results in Fig. 6c, by varying the number of basis vectors used. Experimental results indicate that PAS can significantly improve the sampling quality of DDIM using only the top 2 basis vectors, while employing the top 3 or 4 vectors yields slightly better performance. Notably, the experimental results presented in Fig. 6c exhibit the same trend as those in Fig. 2a, further validating that the sampling trajectory of DPMs lies in a low-dimensional subspace. Four basis vectors suffice to span the sampling trajectory space, enabling PAS to achieve minimal training costs and learnable param-

eters compared to other training-based algorithms.

Number of trajectories. In Fig. 6d, we vary the number of ground truth trajectories from 500 to 20k. We find that learning coordinates from as few as 500 trajectories can significantly enhance the sampling quality of DDIM. This demonstrates that the sampling trajectories of all samples exhibit *strong consistent geometric characteristics*, specifically the “S”-shaped truncation error. This also explains why a set of coordinates can effectively adapt to all samples within a single dataset. However, increasing the number of trajectories generally results in more generalized learned coordinates, with 5k trajectories being the optimal balance.

5. Conclusion

In this paper, we introduced a novel training paradigm, *PAS*, for accelerating DPMs with minimal training costs and learnable parameters. Our key strategy is to obtain a few basis vectors via PCA, and then learn their low-dimensional coordinates to correct the high-dimensional sampling direction vectors. Moreover, based on the observation that the truncation error of existing fast solvers exhibits an “S”-shape, we design an adaptive search strategy to balance the correction steps, further enhancing sampling efficiency and reducing the number of stored parameters to approximately 10. Extensive experiments on both unconditional and con-

ditional pre-trained DPMs demonstrate that PAS can significantly improve the sampling quality of existing fast solvers, such as DDIM and iPNDM, in a plug-and-play manner.

References

- [1] Fan Bao, Chongxuan Li, Jiacheng Sun, Jun Zhu, and Bo Zhang. Estimating the optimal covariance with imperfect mean in diffusion probabilistic models. In *International Conference on Machine Learning*, pages 1555–1584. PMLR, 2022. 6, 1
- [2] Fan Bao, Chongxuan Li, Jun Zhu, and Bo Zhang. Analytic-dpm: an analytic estimate of the optimal reverse variance in diffusion probabilistic models. In *International Conference on Learning Representations*, 2022. 1
- [3] James Betker, Gabriel Goh, Li Jing, Tim Brooks, Jianfeng Wang, Linjie Li, Long Ouyang, Juntang Zhuang, Joyce Lee, Yufei Guo, et al. Improving image generation with better captions. *Computer Science*. <https://cdn.openai.com/papers/dall-e-3.pdf>, 2(3):8, 2023. 1
- [4] Defang Chen, Zhenyu Zhou, Can Wang, Chunhua Shen, and Siwei Lyu. On the trajectory regularity of ode-based diffusion sampling. In *Forty-first International Conference on Machine Learning*, 2024. 1
- [5] Mostafa Dehghani, Basil Mustafa, Josip Djolonga, Jonathan Heek, Matthias Minderer, Mathilde Caron, Andreas Steiner, Joan Puigcerver, Robert Geirhos, Ibrahim Alabdulmohsin, et al. Patch n’pack: Navit, a vision transformer for any aspect ratio and resolution. In *Proceedings of the 37th International Conference on Neural Information Processing Systems*, pages 2252–2274, 2023. 1
- [6] Jia Deng, Wei Dong, Richard Socher, Li-Jia Li, Kai Li, and Li Fei-Fei. Imagenet: A large-scale hierarchical image database. In *2009 IEEE conference on computer vision and pattern recognition*, pages 248–255. Ieee, 2009. 6, 7, 1, 3, 5, 8
- [7] Prafulla Dhariwal and Alexander Nichol. Diffusion models beat gans on image synthesis. *Advances in neural information processing systems*, 34:8780–8794, 2021. 1
- [8] Ian Goodfellow, Jean Pouget-Abadie, Mehdi Mirza, Bing Xu, David Warde-Farley, Sherjil Ozair, Aaron Courville, and Yoshua Bengio. Generative adversarial nets. *Advances in neural information processing systems*, 27, 2014. 1
- [9] Martin Heusel, Hubert Ramsauer, Thomas Unterthiner, Bernhard Nessler, and Sepp Hochreiter. Gans trained by a two time-scale update rule converge to a local nash equilibrium. *Advances in neural information processing systems*, 30, 2017. 6
- [10] Jonathan Ho, Ajay Jain, and Pieter Abbeel. Denoising diffusion probabilistic models. *Advances in neural information processing systems*, 33:6840–6851, 2020. 1, 2
- [11] Yi-Ting Hsiao, Siavash Khodadadeh, Kevin Duarte, Wei-An Lin, Hui Qu, Mingi Kwon, and Ratheesh Kalarot. Plug-and-play diffusion distillation. In *Proceedings of the IEEE/CVF Conference on Computer Vision and Pattern Recognition*, pages 13743–13752, 2024. 6, 1
- [12] Tero Karras, Samuli Laine, and Timo Aila. A style-based generator architecture for generative adversarial networks. In *Proceedings of the IEEE/CVF conference on computer vision and pattern recognition*, pages 4401–4410, 2019. 6, 7, 1, 2, 3, 4, 5
- [13] Tero Karras, Miika Aittala, Timo Aila, and Samuli Laine. Elucidating the design space of diffusion-based generative models. *Advances in neural information processing systems*, 35:26565–26577, 2022. 1, 2, 3, 4, 6, 7, 5
- [14] Bo-Kyeong Kim, Hyoung-Kyu Song, Thibault Castells, and Shinkook Choi. Bk-sdm: A lightweight, fast, and cheap version of stable diffusion. *arXiv preprint arXiv:2305.15798*, 2023. 6, 1
- [15] Dongjun Kim, Yeongmin Kim, Se Jung Kwon, Wanmo Kang, and Il-Chul Moon. Refining generative process with discriminator guidance in score-based diffusion models. In *International Conference on Machine Learning*, pages 16567–16598. PMLR, 2023. 6, 1
- [16] Diederik P Kingma and Max Welling. Auto-encoding variational bayes. *arXiv preprint arXiv:1312.6114*, 2013. 1
- [17] Peter E Kloeden, Eckhard Platen, Peter E Kloeden, and Eckhard Platen. *Stochastic differential equations*. Springer, 1992. 3, 4, 5, 6
- [18] Alex Krizhevsky, Geoffrey Hinton, et al. Learning multiple layers of features from tiny images. *Technical Report*, 2009. 6, 7, 1, 2, 3, 4, 5
- [19] Lijiang Li, Huixia Li, Xiawu Zheng, Jie Wu, Xuefeng Xiao, Rui Wang, Min Zheng, Xin Pan, Fei Chao, and Rongrong Ji. Autodiffusion: Training-free optimization of time steps and architectures for automated diffusion model acceleration. In *Proceedings of the IEEE/CVF International Conference on Computer Vision*, pages 7105–7114, 2023. 1
- [20] Tsung-Yi Lin, Michael Maire, Serge Belongie, James Hays, Pietro Perona, Deva Ramanan, Piotr Dollár, and C Lawrence Zitnick. Microsoft coco: Common objects in context. In *Computer Vision—ECCV 2014: 13th European Conference, Zurich, Switzerland, September 6–12, 2014, Proceedings, Part V 13*, pages 740–755. Springer, 2014. 6
- [21] Luping Liu, Yi Ren, Zhijie Lin, and Zhou Zhao. Pseudo numerical methods for diffusion models on manifolds. In *International Conference on Learning Representations*, 2022. 1, 3, 6, 7, 2, 4, 5, 8, 9
- [22] Xingchao Liu, Chengyue Gong, et al. Flow straight and fast: Learning to generate and transfer data with rectified flow. In *The Eleventh International Conference on Learning Representations*, 2022. 1, 6
- [23] Cheng Lu, Yuhao Zhou, Fan Bao, Jianfei Chen, Chongxuan Li, and Jun Zhu. Dpm-solver: a fast ode solver for diffusion probabilistic model sampling in around 10 steps. In *Proceedings of the 36th International Conference on Neural Information Processing Systems*, pages 5775–5787, 2022. 1, 2, 3, 6, 7, 4
- [24] Cheng Lu, Yuhao Zhou, Fan Bao, Jianfei Chen, Chongxuan Li, and Jun Zhu. Dpm-solver++: Fast solver for guided sampling of diffusion probabilistic models. *arXiv preprint arXiv:2211.01095*, 2022. 1, 2, 3, 6, 7
- [25] Xinyin Ma, Gongfan Fang, and Xinchao Wang. Deepcache: Accelerating diffusion models for free. In *Proceedings of the IEEE/CVF Conference on Computer Vision and Pattern Recognition*, pages 15762–15772, 2024. 1

- [26] Byeonghu Na, Yeongmin Kim, Minsang Park, Donghyeok Shin, Wanmo Kang, and Il-chul Moon. Diffusion rejection sampling. In *Forty-first International Conference on Machine Learning*, 2024. 6, 1
- [27] Bernt Øksendal. *Stochastic differential equations: an introduction with applications*. Springer Science & Business Media, 2013. 2
- [28] Bernt Øksendal and Bernt Øksendal. *Stochastic differential equations*. Springer, 2003. 2
- [29] William Peebles and Saining Xie. Scalable diffusion models with transformers. In *Proceedings of the IEEE/CVF International Conference on Computer Vision*, pages 4195–4205, 2023. 1
- [30] Herbert Robbins and Sutton Monro. A stochastic approximation method. *The annals of mathematical statistics*, pages 400–407, 1951. 4
- [31] Robin Rombach, Andreas Blattmann, Dominik Lorenz, Patrick Esser, and Björn Ommer. High-resolution image synthesis with latent diffusion models. In *Proceedings of the IEEE/CVF conference on computer vision and pattern recognition*, pages 10684–10695, 2022. 1, 6, 3, 4, 5
- [32] Tim Salimans and Jonathan Ho. Progressive distillation for fast sampling of diffusion models. In *International Conference on Learning Representations*, 2022. 1, 2, 3, 6
- [33] Andy Shih, Suneel Belkhale, Stefano Ermon, Dorsa Sadigh, and Nima Anari. Parallel sampling of diffusion models. In *Proceedings of the 37th International Conference on Neural Information Processing Systems*, pages 4263–4276, 2023. 1
- [34] Chenyang Si, Ziqi Huang, Yuming Jiang, and Ziwei Liu. Free: Free lunch in diffusion u-net. In *Proceedings of the IEEE/CVF Conference on Computer Vision and Pattern Recognition*, pages 4733–4743, 2024. 1
- [35] Jascha Sohl-Dickstein, Eric Weiss, Niru Maheswaranathan, and Surya Ganguli. Deep unsupervised learning using nonequilibrium thermodynamics. In *International conference on machine learning*, pages 2256–2265. PMLR, 2015. 1, 2
- [36] Jiaming Song, Chenlin Meng, and Stefano Ermon. Denoising diffusion implicit models. *arXiv preprint arXiv:2010.02502*, 2020. 1, 2, 6, 7, 3, 4, 5, 8, 9
- [37] Kaitao Song, Yichong Leng, Xu Tan, Yicheng Zou, Tao Qin, and Dongsheng Li. Transcormer: Transformer for sentence scoring with sliding language modeling. *Advances in Neural Information Processing Systems*, 35:11160–11174, 2022. 1
- [38] Yang Song and Prafulla Dhariwal. Improved techniques for training consistency models. *arXiv preprint arXiv:2310.14189*, 2023. 8
- [39] Yang Song and Stefano Ermon. Generative modeling by estimating gradients of the data distribution. *Advances in neural information processing systems*, 32, 2019. 1, 2
- [40] Yang Song, Jascha Sohl-Dickstein, Diederik P Kingma, Abhishek Kumar, Stefano Ermon, and Ben Poole. Score-based generative modeling through stochastic differential equations. *arXiv preprint arXiv:2011.13456*, 2020. 1, 2
- [41] Yang Song, Prafulla Dhariwal, Mark Chen, and Ilya Sutskever. Consistency models. In *International Conference on Machine Learning*, pages 32211–32252. PMLR, 2023. 1, 2, 3, 6
- [42] Felix Wimbauer, Bichen Wu, Edgar Schoenfeld, Xiaoliang Dai, Ji Hou, Zijian He, Artsiom Sanakoyeu, Peizhao Zhang, Sam Tsai, Jonas Kohler, et al. Cache me if you can: Accelerating diffusion models through block caching. In *Proceedings of the IEEE/CVF Conference on Computer Vision and Pattern Recognition*, pages 6211–6220, 2024. 1
- [43] Mengfei Xia, Yujun Shen, Changsong Lei, Yu Zhou, Deli Zhao, Ran Yi, Wenping Wang, and Yong-Jin Liu. Towards more accurate diffusion model acceleration with a timestep tuner. In *Proceedings of the IEEE/CVF Conference on Computer Vision and Pattern Recognition*, pages 5736–5745, 2024. 1
- [44] Tianwei Yin, Michaël Gharbi, Richard Zhang, Eli Shechtman, Fredo Durand, William T Freeman, and Taesung Park. One-step diffusion with distribution matching distillation. In *Proceedings of the IEEE/CVF Conference on Computer Vision and Pattern Recognition*, pages 6613–6623, 2024. 1, 6
- [45] Fisher Yu, Ari Seff, Yinda Zhang, Shuran Song, Thomas Funkhouser, and Jianxiong Xiao. Lsun: Construction of a large-scale image dataset using deep learning with humans in the loop. *arXiv preprint arXiv:1506.03365*, 2015. 6, 7, 1, 3, 4, 5, 9
- [46] Junyu Zhang, Daochang Liu, Eunbyung Park, Shichao Zhang, and Chang Xu. Residual learning in diffusion models. In *Proceedings of the IEEE/CVF Conference on Computer Vision and Pattern Recognition*, pages 7289–7299, 2024. 6, 1
- [47] Qinsheng Zhang and Yongxin Chen. Fast sampling of diffusion models with exponential integrator. *Proceedings of Machine Learning Research*, 2023. 1, 3, 6, 7, 2, 4, 5, 8, 9
- [48] Richard Zhang, Phillip Isola, Alexei A Efros, Eli Shechtman, and Oliver Wang. The unreasonable effectiveness of deep features as a perceptual metric. In *Proceedings of the IEEE conference on computer vision and pattern recognition*, pages 586–595, 2018. 8
- [49] Wenliang Zhao, Lujia Bai, Yongming Rao, Jie Zhou, and Jiwen Lu. Unipc: a unified predictor-corrector framework for fast sampling of diffusion models. In *Proceedings of the 37th International Conference on Neural Information Processing Systems*, pages 49842–49869, 2023. 1, 6, 7, 2
- [50] Kaiwen Zheng, Cheng Lu, Jianfei Chen, and Jun Zhu. Dpm-solver-v3: improved diffusion ode solver with empirical model statistics. In *Proceedings of the 37th International Conference on Neural Information Processing Systems*, pages 55502–55542, 2023. 1, 6, 7
- [51] Zhenyu Zhou, Defang Chen, Can Wang, and Chun Chen. Fast ode-based sampling for diffusion models in around 5 steps. In *Proceedings of the IEEE/CVF Conference on Computer Vision and Pattern Recognition*, pages 7777–7786, 2024. 2, 3, 6, 1

Diffusion Sampling Correction via Approximately 10 Parameters

Supplementary Material

A. Related works

Low-cost training. Previous studies [22, 32, 41] have shown that directly learning the mapping between noise and data distributions necessitates high training costs for minimal-step sampling. Recently, several low-cost training methods have been proposed. Kim *et al.* [14] and Hsiao *et al.* [11] explored how to reduce the number of parameters in student models to achieve efficient distillation. Bao *et al.* [1], Kim *et al.* [15], and Na *et al.* [26] corrected errors arising during the sampling process by training smaller neural networks. Zhang *et al.* [46] suggested training the neural network only for the last step of sampling to eliminate accumulated residuals, thereby reducing training costs. Zhou *et al.* [51] optimized training expenses by using the Mean Value Theorem to reduce the output dimensions of neural networks. However, these methods typically still require training a new, relatively small neural network. Unlike these approaches, the proposed PAS method requires learning only a few sets of coordinates, which results in *minimized learnable parameters and training costs*.

Plug-and-play acceleration. Numerous studies [4, 19, 25, 33, 34, 42, 43] have explored ways to accelerate existing fast solvers, such as DDIM [36], DPM-Solver [23, 24], PNDM [21], and DEIS [47]. Specifically, Ma *et al.* [25] and Wimbauer *et al.* [42] reduced the computational load of neural networks by caching their low-level features. Li *et al.* [19] and Chen *et al.* [4] suggested searching for optimal sampling schedules to enhance sampling quality in fewer steps. Shih *et al.* [33] proposed utilizing more computational resources and implementing parallelized sampling processes to shorten sampling times. *Orthogonal to these studies*, the proposed PAS method introduces a new orthogonal axis for accelerated sampling in DPMs, which can be further integrated with these approaches to enhance the sampling efficiency of existing fast solvers.

B. Training details and discussion

In this section, we provide training details regarding the PAS correction for different solvers (including DDIM [36] and iPNDM [21, 47]) across various datasets. Unless mentioned in the ablation experiments or special notes, all experimental settings related to training are based on what is described in this section. First, we outline some common experimental settings: we use Heun’s 2nd solver from EDM [13] with 100 NFE to generate ground truth trajectories. We uniformly apply four orthogonal unit basis vectors (where $\mathbf{u}_1 = d_{t_{i+1}} / \|d_{t_{i+1}}\|_2$) to correct the sampling directions. Notably, for the PCA process in Eq. (10), we

| Method (+ PAS) | LR | Loss | Trajectory | Tolerance |
|--------------------------------------|-----------|-------|------------|-----------|
| CIFAR10 32×32 [18] | | | | |
| DDIM [36] | 10^{-2} | L_1 | 10k | 10^{-2} |
| iPNDM [21, 47] | 1 | L_1 | 5k | 10^{-4} |
| FFHQ 64×64 [12] | | | | |
| DDIM [36] | 10^{-2} | L_1 | 10k | 10^{-2} |
| iPNDM [21, 47] | 10^{-3} | L_1 | 5k | 10^{-4} |
| ImageNet 64×64 [6] | | | | |
| DDIM [36] | 10^{-2} | L_1 | 10k | 10^{-2} |
| iPNDM [21, 47] | 10^{-3} | L_2 | 5k | 10^{-4} |
| LSUN Bedroom 256×256 [45] | | | | |
| DDIM [36] | 10^{-2} | L_1 | 5k | 10^{-2} |
| iPNDM [21, 47] | 10^{-2} | L_1 | 5k | 10^{-4} |
| Stable Diffusion 512×512 [31] | | | | |
| DDIM [36] | 10 | L_1 | 5k | 10^{-2} |

Table 4. Training settings for learning rate (LR), loss function (Loss), number of ground truth trajectories (Trajectory), and tolerance τ (Tolerance) when applying PAS to correct DDIM [36] and iPNDM [21, 47] solvers across various datasets and pre-trained models.

utilize the `torch.pca_lowrank` function to obtain the basis vectors, as it offers a faster computation speed compared to `torch.svd`. Second, other hyperparameters such as learning rate, loss function, the number of ground truth trajectories, and tolerance τ are specified in Tab. 4.

Regarding the aforementioned hyperparameter settings, we conducted extensive ablation experiments in Sec. 4.3 and Appendix C.2 to elucidate the rationale behind these choices. Furthermore, we note that the impact of hyperparameter settings on the correction of DDIM is not a critical factor, as DDIM exhibits substantial truncation error; regardless of how hyperparameters are configured, PAS significantly enhances the sampling quality of DDIM. In contrast, since the iPNDM solver’s sampling quality is already relatively high, certain hyperparameters need to be adjusted when using PAS to achieve better FID scores. Nevertheless, due to the extremely low training cost of PAS (requiring only 0~2 minutes on a single NVIDIA A100 GPU for the CIFAR10 and 10~20 minutes for larger datasets at a resolution of 256), we can *easily* conduct hyperparameter searches. Coincidentally, the final training loss can serve as a reference for assessing the effectiveness of hyperparame-

| Method | NFE | | | | | | |
|---------------------------|--------------|--------------|--------------|-------------|-------------|-------------|-------------|
| | 4 | 5 | 6 | 7 | 8 | 9 | 10 |
| CIFAR10 32×32 [18] | | | | | | | |
| DDIM [36] | 66.76 | 49.68 | 35.63 | 27.93 | 22.32 | 18.43 | 15.69 |
| DDIM + PAS (Ours) | 41.14 | 17.13 | 12.11 | 11.77 | 7.07 | 5.56 | 4.37 |
| Heun’s 2nd [13] | 319.87 | \ | 99.74 | \ | 38.06 | \ | 15.93 |
| DPM-Solver-2 [23] | 145.98 | \ | 60.00 | \ | 10.30 | \ | 5.01 |
| DPM-Solver++(3M) [24] | 50.39 | 31.65 | 17.89 | 11.30 | 8.30 | 6.45 | 5.16 |
| DEIS-tAB3 [47] | 47.13 | 17.65 | 11.84 | 10.89 | 6.82 | 6.21 | 5.64 |
| UniPC(3M) [49] | 49.79 | 31.44 | 17.74 | 11.24 | 8.42 | 6.69 | 5.31 |
| iPNDM [21, 47] | 29.49 | 16.55 | 9.74 | 6.92 | 5.23 | 4.33 | 3.69 |
| iPNDM + PAS (Ours) | 27.59 | 13.61 | 7.47 | 5.59 | 3.87 | 3.17 | 2.84 |
| FFHQ 64×64 [12] | | | | | | | |
| DDIM [36] | 57.48 | 43.92 | 35.21 | 28.86 | 24.38 | 21.01 | 18.37 |
| DDIM + PAS (Ours) | 39.09 | 29.07 | 17.63 | 12.47 | 8.16 | 8.26 | 5.61 |
| Heun’s 2nd [13] | 344.87 | \ | 142.39 | \ | 57.21 | \ | 29.54 |
| DPM-Solver-2 [23] | 238.57 | \ | 83.17 | \ | 22.84 | \ | 9.46 |
| DPM-Solver++(3M) [24] | 39.50 | 23.50 | 14.93 | 11.04 | 9.58 | 8.36 | 6.96 |
| DEIS-tAB3 [47] | 35.34 | 19.47 | 11.61 | 11.70 | 8.64 | 7.72 | 7.07 |
| UniPC(3M) [49] | 38.60 | 22.82 | 14.30 | 10.90 | 10.07 | 9.00 | 7.39 |
| iPNDM [21, 47] | 29.07 | 17.26 | 11.31 | 8.56 | 6.82 | 5.71 | 4.95 |
| iPNDM + PAS (Ours) | 41.89 | 15.89 | 10.29 | 7.59 | 5.85 | 4.88 | 4.28 |

Table 5. Sample quality measured by Fréchet Inception Distance (FID \downarrow) on CIFAR10 32×32 [18], FFHQ 64×64 [12] datasets, varying the number of function evaluations (NFE) from 4 to 10. “\” indicates missing data due to the inherent characteristics of the algorithm.

ter choices.

Regarding hyperparameter search recommendations, for solvers with significant truncation errors (*e.g.*, DDIM [36]), we suggest using a learning rate of 10^{-2} , the L_1 loss function, 5k ground truth trajectories, and a tolerance τ of 10^{-2} , which generally applies to all datasets. Conversely, for solvers with smaller truncation errors (*e.g.*, iPNDM [21, 47]), we recommend conducting a learning rate search from 10^{-4} to 10 for different datasets, while fixing the L_1 loss function, using 5k ground truth trajectories, setting the tolerance τ to 10^{-4} .

It is important to emphasize that the mainstream evaluation metric for the quality of generated samples is FID; however, there is no corresponding FID loss function. Therefore, when training coordinates using the L_1 or L_2 loss functions, even if the FID score does not improve during the correction of the iPNDM solver, the L_1 and L_2 metrics show improvement, as demonstrated in Tab. 11. This further corroborates the effectiveness of the proposed PAS as a plug-and-play correction algorithm.

C. Additional experiment results

In this section, we present additional experimental results on NFE, corrected time points, the order of iPNDM, ablation studies, and visualization studies. Except for the ablation experiments and specific clarifications, the experimen-

tal setup and training details are consistent with Sec. 4 and Appendix B.

C.1. Additional results on NFE and corrected time points

In this section, we first extend the FID results on the CIFAR10 32×32 [18] and FFHQ 64×64 [12] datasets for more values of NFE $\in \{4, 5, 6, 7, 8, 9, 10\}$. The results of PAS correcting DDIM [36] and iPNDM [21, 47] with the order of 3 are shown in Tab. 5 (for more results regarding the order of iPNDM, see Appendix C.3). The results indicate that PAS can significantly improve the sampling quality of DDIM and iPNDM across different NFE.

Additionally, in Tab. 6, we present the time points corrected by PAS for the DDIM and iPNDM solvers across various datasets, which correspond to Tabs. 2 and 3. From Tab. 6, it can be observed that the DDIM, which has a large truncation error, requires correction of more sampling steps, while the iPNDM, which exhibits a smaller truncation error, requires relatively fewer correction steps, which *aligns with our intuition*. Overall, PAS only needs to correct 1~5 time points, which corresponds to requiring only 4~20 learnable parameters, to significantly enhance the sampling quality of the baseline solvers. This validates the effectiveness of PAS as an acceleration algorithm with extremely low training costs.

| Method | NFE | | | |
|--------------------------------------|-------|---------|---------|-----------|
| | 5 | 6 | 8 | 10 |
| CIFAR10 32×32 [18] | | | | |
| DDIM + PAS | 3,1 | 4,2,1 | 5,3,2 | 6,4,2 |
| iPNDM + PAS | 2 | 3 | 3,1 | 4,2 |
| FFHQ 64×64 [12] | | | | |
| DDIM + PAS | 3,2,1 | 4,3,1 | 5,4,2,1 | 7,5,3,2 |
| iPNDM + PAS | 3 | 3,1 | 4,2 | 4,2 |
| ImageNet 64×64 [6] | | | | |
| DDIM + PAS | 3,2,1 | 4,3,1 | 5,4,2,1 | 7,5,4,2,1 |
| iPNDM + PAS | 3 | 3 | 4 | 5 |
| LSUN Bedroom 256×256 [45] | | | | |
| DDIM + PAS | 4,3,1 | 5,4,2 | 6,5,3,2 | 8,7,5,4 |
| iPNDM + PAS | 4,2 | 5,3,2,1 | 6,4,3,1 | 8,6,4,3 |
| Stable Diffusion 512×512 [31] | | | | |
| DDIM + PAS | 3,2,1 | 2,1 | 2,1 | 1 |

Table 6. Time points i are corrected by PAS for the DDIM [36] and iPNDM [21, 47] solvers, as corresponding to Tabs. 2 and 3, ranging from NFE (N) to 1.

C.2. Additional ablation study results

In this section, we first supplement additional ablation experiments concerning the adaptive search. Subsequently, we provide further ablation experiments on learning rate, tolerance τ , and solvers for trajectory generation.

More results on adaptive search. Regarding the adaptive search strategy, we first supplement the specific FID values corresponding to Fig. 6a on the CIFAR10 32×32 [18] dataset, as shown in Tab. 7. Additionally, in Tab. 7, we also provide experimental results on the FFHQ 64×64 [12] dataset, using PAS alongside PAS without the adaptive search strategy (PAS(-AS)) to correct DDIM [36]. Consistent with the results in Fig. 6a, when the adaptive search strategy is not employed—specifically when PCA-based sampling correction is applied at each time step—the sampling quality is inferior to that of the baseline DDIM. Furthermore, the absence of the adaptive search strategy results in increased computational time, as PCA-based sampling correction is required at each step. In Sec. 3.3, we described the motivation and process of the proposed adaptive search strategy. We analyzed the ground truth trajectory transitioning from a straight line to a curve, and ultimately back to a straight line. The adaptive search is designed to correct the errors in the large curvature regions of the sampling trajectory. In the straight linear segments, the errors introduced by the existing fast solvers (*e.g.*, DDIM) are negligible, and the application of PCA-based sampling correction does not provide any further error adjustment. Instead, it in-

| Method | NFE | | | |
|---------------------------|--------------|--------------|-------------|-------------|
| | 5 | 6 | 8 | 10 |
| CIFAR10 32×32 [18] | | | | |
| DDIM [36] | 49.68 | 35.63 | 22.32 | 15.69 |
| DDIM + PAS (-AS) | 132.12 | 139.48 | 143.54 | 120.32 |
| DDIM + PAS | 17.13 | 12.11 | 7.07 | 4.37 |
| FFHQ 64×64 [12] | | | | |
| DDIM [36] | 43.92 | 35.21 | 24.38 | 18.37 |
| DDIM + PAS (-AS) | 78.10 | 98.84 | 98.67 | 93.62 |
| DDIM + PAS | 29.07 | 17.63 | 8.16 | 5.61 |

Table 7. Ablation study regarding adaptive search conducted on the CIFAR10 32×32 [18] and FFHQ 64×64 [12] datasets, employing PAS alongside PAS without adaptive search (PAS (-AS)) to correct DDIM [36]. We report the Fréchet Inception Distance (FID \downarrow) score, varying the number of function evaluations (NFE).

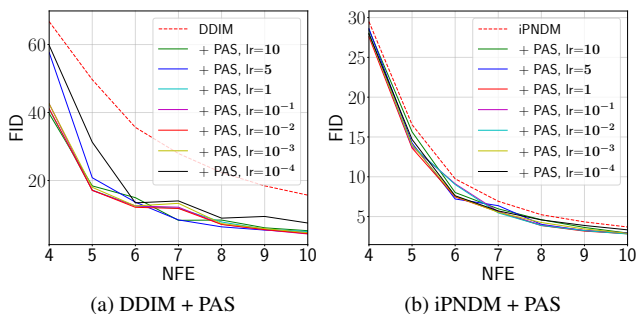


Figure 7. Ablation study regarding learning rate conducted on the CIFAR10 32×32 [18], utilizing PAS to correct DDIM [36] and iPNDM [21, 47] solvers. We report the Fréchet Inception Distance (FID \downarrow) score, varying the number of function evaluations (NFE).

roduces biases on other basis vectors, leading to a decline in sampling quality. Therefore, it is essential to combine the adaptive search strategy with PCA-based sampling correction, specifically to correct truncation errors in regions of high curvature in the sampling trajectory. Combining Fig. 6a and Tab. 7, further validates the necessity and effectiveness of the proposed overall algorithm, PCA-based Adaptive Search (PAS).

Learning rate. In Fig. 7, we present the ablation results of the PAS correcting DDIM [36] and iPNDM [21, 47] with the order of 3 on the CIFAR10 32×32 [18] dataset. We varied the learning rate from 10^{-4} to 10. The results demonstrate that, regardless of the learning rate setting, PAS significantly improves the sampling quality of both DDIM and iPNDM on the CIFAR10, and further exploration exhibits slightly better sampling performance.

Tolerance τ . In Sec. 3.3, we designed an adaptive search strategy to enhance the overall performance of PCA-based sampling correction. This adaptive search strategy relies

| Method | τ | NFE | | | |
|---------------------------|-----------|-------|-------|-------|-------|
| | | 5 | 6 | 8 | 10 |
| CIFAR10 32×32 [18] | | | | | |
| DDIM [36] | \ | 49.68 | 35.63 | 22.32 | 15.69 |
| DDIM + PAS | 10^{-1} | 49.68 | 35.63 | 22.32 | 15.69 |
| DDIM + PAS | 10^{-2} | 17.13 | 12.11 | 7.07 | 4.37 |
| DDIM + PAS | 10^{-3} | 17.13 | 12.11 | 7.07 | 4.37 |
| DDIM + PAS | 10^{-4} | 17.13 | 12.11 | 7.07 | 4.37 |
| iPNDM [21, 47] | \ | 16.55 | 9.74 | 5.23 | 3.69 |
| iPNDM + PAS | 10^{-2} | 13.61 | 9.74 | 5.23 | 3.69 |
| iPNDM + PAS | 10^{-3} | 13.61 | 7.47 | 3.87 | 2.91 |
| iPNDM + PAS | 10^{-4} | 13.61 | 7.47 | 3.87 | 2.84 |

Table 8. Ablation study regarding tolerance τ conducted on the CIFAR10 32×32 [18], utilizing PAS to correct DDIM [36] and iPNDM [21, 47] solvers. We report the Fréchet Inception Distance (FID \downarrow) score, varying the number of function evaluations (NFE).

| Method | Solver | NFE | | | |
|---------------------------|--------|--------------|--------------|-------------|-------------|
| | | 5 | 6 | 8 | 10 |
| CIFAR10 32×32 [18] | | | | | |
| DDIM [36] | \ | 49.68 | 35.63 | 22.32 | 15.69 |
| DDIM + PAS | Heun | 17.13 | 12.11 | 7.07 | 4.37 |
| DDIM + PAS | DDIM | 17.10 | 12.44 | 6.97 | 4.87 |
| DDIM + PAS | DPM | 17.12 | 12.10 | 7.10 | 4.40 |
| FFHQ 64×64 [12] | | | | | |
| DDIM [36] | \ | 43.92 | 35.21 | 24.38 | 18.37 |
| DDIM + PAS | Heun | 29.07 | 17.63 | 8.16 | 5.61 |
| DDIM + PAS | DDIM | 30.49 | 15.26 | 8.65 | 6.37 |
| DDIM + PAS | DPM | 29.11 | 17.58 | 8.12 | 5.64 |

Table 9. Ablation study regarding solvers for generating ground truth trajectories, including Heun’s 2nd (Heun) [13], DDIM [36], and DPM-Solver-2 (DPM) [23], conducted on the CIFAR10 32×32 [18] and FFHQ 64×64 [12]. We report the Fréchet Inception Distance (FID \downarrow) score, employing PAS to correct DDIM [36], varying the number of function evaluations (NFE).

on the condition $\mathcal{L}_2 - (\mathcal{L}_1 + \tau) > 0$. Therefore, we further investigate the impact of the tolerance τ on the adaptive search strategy. It is important to emphasize that the adaptive search strategy is aimed at correcting the sections of the sampling trajectory with large curvature, while the tolerance τ serves as the criterion for determining whether the current sampling state has reached a region of large curvature in the trajectory. Consequently, the tolerance τ is initially treated as a hyperparameter to indicate the time point at which correction should commence, while subsequent time points have their tolerance τ fixed at 10^{-4} . We adjusted the tolerance τ for the initial correction point from 10^{-1} to 10^{-4} , and the experimental results on the CIFAR10

32×32 [18] dataset are presented in Tab. 8. The experimental findings indicate that PAS is not sensitive to the configuration of the hyperparameter tolerance τ . PAS consistently demonstrates a significant improvement in the sampling quality of DDIM [36] and iPNDM [21, 47] solvers with tolerance τ ranging from 10^{-2} to 10^{-4} . Lastly, we recommend setting the tolerance τ to 10^{-2} for solvers with substantial truncation error (e.g., DDIM), while for solvers with relatively smaller truncation error (e.g., iPNDM), the tolerance τ should be set to 10^{-4} .

Solvers for trajectory generation We investigated the impact of solver selection for generating ground truth trajectories on the performance of PAS using the CIFAR10 32×32 [18] and FFHQ 64×64 [12] datasets. We employed Heun’s 2nd [13], DDIM [36], and DPM-Solver-2 [23] solvers with 100 NFE to generate 10k trajectories for training the PAS to correct the DDIM solver, as shown in Tab. 9. Our findings indicate that the choice of solver for generating ground truth trajectories has negligible impact on the performance of PAS. This suggests that regardless of the solver used, a sufficient number of NFE (e.g., 100 NFE) enables the solving process to approximate the ground truth trajectories closely. Therefore, we simply fixed Heun’s 2nd solver for all experiments.

C.3. Additional results on the order of iPNDM

In this section, we discuss why we mainly chose to apply PAS correcting iPNDM with the order of 3 in Tab. 2. First, we evaluated the sampling quality of iPNDM by adjusting its order on the CIFAR10 32×32 [18], LSUN Bedroom 256×256 [45] datasets, and Stable Diffusion [31], as shown in Tabs. 10 and 11. We found that increasing the order of

| Method | Order | NFE | | | |
|--------------------------------------|-------|--------------|--------------|--------------|--------------|
| | | 5 | 6 | 8 | 10 |
| LSUN Bedroom 256×256 [45] | | | | | |
| iPNDM [21, 47] | 1 | 34.34 | 25.25 | 15.71 | 11.42 |
| iPNDM [21, 47] | 2 | 18.15 | 12.90 | 7.98 | 6.17 |
| iPNDM [21, 47] | 3 | 16.57 | 10.83 | 6.18 | 4.92 |
| iPNDM [21, 47] | 4 | 26.65 | 20.72 | 11.77 | 5.56 |
| iPNDM + PAS | 2 | 15.48 | 10.24 | 6.67 | 5.14 |
| iPNDM + PAS | 3 | 18.59 | 12.06 | 5.92 | 4.84 |
| Stable Diffusion 512×512 [31] | | | | | |
| iPNDM [21, 47] | 3 | 22.31 | 17.21 | 13.60 | 13.71 |
| iPNDM [21, 47] | 4 | 28.12 | 25.69 | 20.68 | 16.45 |
| DDIM [36] | \ | 23.42 | 20.08 | 17.72 | 16.56 |
| DDIM + PAS | \ | 17.70 | 15.93 | 14.74 | 14.23 |

Table 10. Sample quality measured by Fréchet Inception Distance (FID \downarrow) on the LSUN Bedroom 256×256 [45] dataset and Stable Diffusion [31], varying the order of iPNDM [21, 47].

| Method | Order | Metrics | NFE | | | | | | |
|--|-------|--------------|-------|-------|-------|-------|-------|-------|-------|
| | | | 4 | 5 | 6 | 7 | 8 | 9 | 10 |
| CIFAR10 32×32 [18], Fréchet Inception Distance (FID↓) metric | | | | | | | | | |
| iPNDM [21, 47] | 1 | FID↓ | 66.76 | 49.68 | 35.63 | 27.93 | 22.32 | 18.43 | 15.69 |
| iPNDM + PAS (Ours) | 1 | FID↓ | 41.14 | 17.13 | 12.11 | 11.77 | 7.07 | 5.56 | 4.37 |
| iPNDM [21, 47] | 2 | FID↓ | 39.02 | 25.24 | 16.19 | 11.85 | 9.08 | 7.39 | 6.18 |
| iPNDM + PAS (Ours) | 2 | FID↓ | 33.54 | 16.59 | 9.77 | 5.87 | 4.51 | 3.55 | 3.01 |
| iPNDM [21, 47] | 3 | FID↓ | 29.49 | 16.55 | 9.74 | 6.92 | 5.23 | 4.33 | 3.69 |
| iPNDM + PAS (Ours) | 3 | FID↓ | 27.59 | 13.61 | 7.47 | 5.59 | 3.87 | 3.17 | 2.84 |
| iPNDM [21, 47] | 4 | FID↓ | 24.82 | 13.58 | 7.05 | 5.08 | 3.69 | 3.17 | 2.77 |
| iPNDM + PAS (Ours) | 4 | FID↓ | 25.79 | 13.74 | 7.95 | 5.89 | 4.66 | 3.42 | 2.97 |
| CIFAR10 32×32 [18], L_2 (MSE) and L_1 metrics | | | | | | | | | |
| iPNDM [21, 47] | 4 | L_2 (MSE)↓ | 0.027 | 0.016 | 0.009 | 0.006 | 0.004 | 0.003 | 0.002 |
| iPNDM + PAS (Ours) | 4 | L_2 (MSE)↓ | 0.020 | 0.014 | 0.009 | 0.006 | 0.004 | 0.003 | 0.002 |
| iPNDM [21, 47] | 4 | L_1 ↓ | 0.126 | 0.089 | 0.063 | 0.047 | 0.037 | 0.030 | 0.025 |
| iPNDM + PAS (Ours) | 4 | L_1 ↓ | 0.100 | 0.078 | 0.059 | 0.047 | 0.037 | 0.031 | 0.026 |

Table 11. Sample quality measured by Fréchet Inception Distance (FID↓), L_2 (MSE)↓, and L_1 ↓ metrics on the CIFAR10 32×32 [18] dataset, varying the order of iPNDM [21, 47]. The L_2 (MSE) and L_1 metrics were evaluated against Heun’s 2nd solver [13] with 100 NFE, using 50k samples.

iPNDM does not always enhance sampling quality. Particularly on high-resolution datasets, optimal sampling quality is often not achieved at iPNDM with the order of 4; in comparison, iPNDM with order 3 demonstrates better average performance. Therefore, we mainly selected PAS to correct the iPNDM with the order of 3 in Tab. 2.

Furthermore, on low-resolution datasets, such as CIFAR10 32×32 [18], iPNDM with the order of 4 displays the best performance. Consequently, we employed PAS to correct its truncation error; however, we observed no improvement in its FID score. Nevertheless, the iPNDM corrected by PAS with the order of 4 performs better in terms of L_1 and L_2 metrics, as indicated in Tab. 11. This phenomenon may be attributed to the fact that PAS uses L_1 or L_2 loss functions during training, and when the solver’s sampling quality is already relatively satisfactory, *there is not always consistency between the L_1 , L_2 metrics and the FID score.*

C.4. Additional visualize study results

We present additional visual sampling results using Stable Diffusion v1.4 [31], as shown in Fig. 8. Furthermore, more visual results on the CIFAR10 32×32 [18], FFHQ 64×64 [12], ImageNet 64×64 [6], and LSUN Bedroom 256×256 [45] datasets with NFE of 6 and 10 are displayed in Figs. 9 to 16. These visual results demonstrate that the samples generated by PAS exhibit *higher quality and richer details* compared to the corresponding baselines.

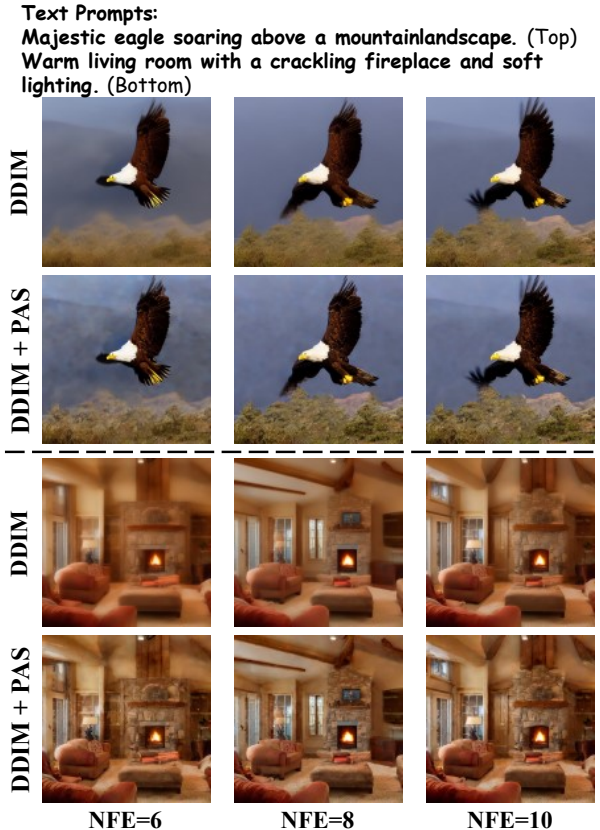


Figure 8. Random samples by DDIM [36] with and without the proposed PAS on Stable Diffusion v1.4 [31] with a guidance scale of 7.5.

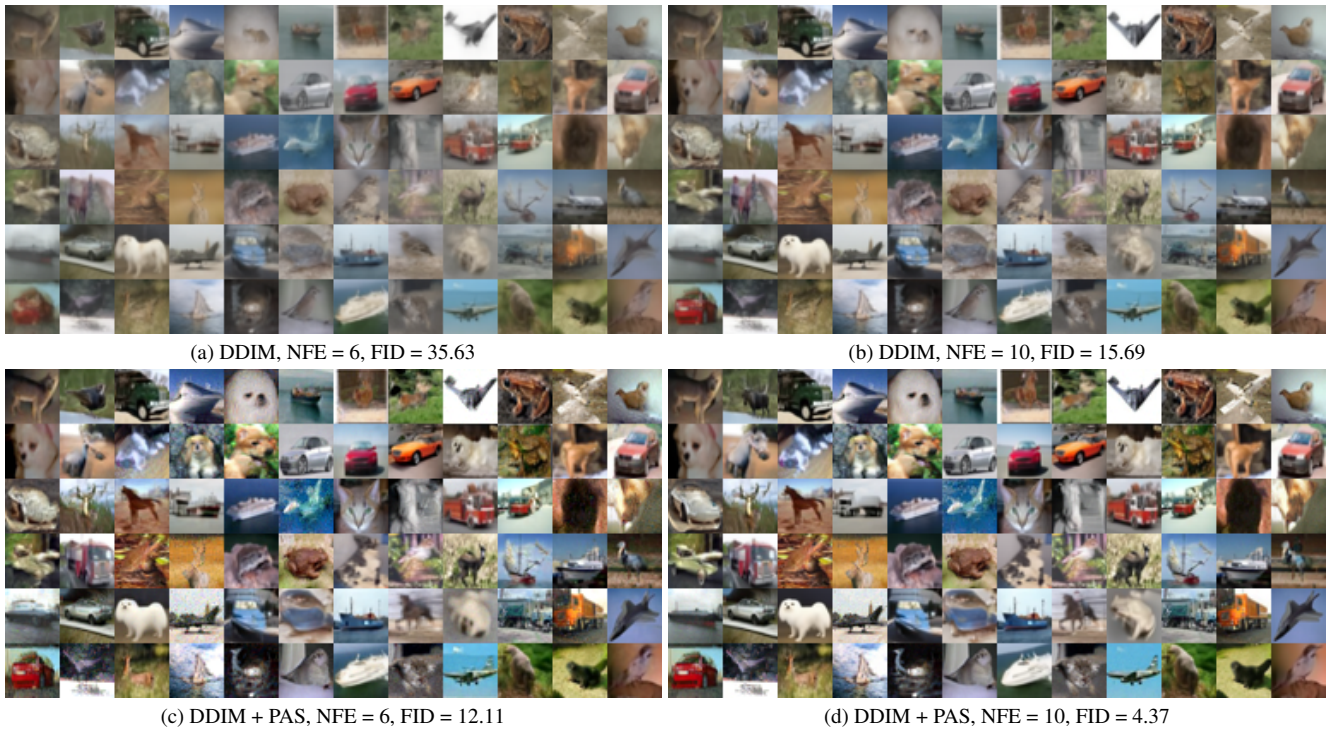


Figure 9. Random samples by DDIM [36] with and without the proposed PAS on CIFAR10 32×32 [18].



Figure 10. Random samples by iPNDM [21, 47] with and without the proposed PAS on CIFAR10 32×32 [18].



(a) DDIM, NFE = 6, FID = 35.21

(b) DDIM, NFE = 10, FID = 18.37



(c) DDIM + PAS, NFE = 6, FID = 17.63

(d) DDIM + PAS, NFE = 10, FID = 5.61

Figure 11. Random samples by DDIM [36] with and without the proposed PAS on FFHQ 64×64 [12].



(a) iPNDM, NFE = 6, FID = 11.31

(b) iPNDM, NFE = 10, FID = 4.95



(c) iPNDM + PAS, NFE = 6, FID = 10.29

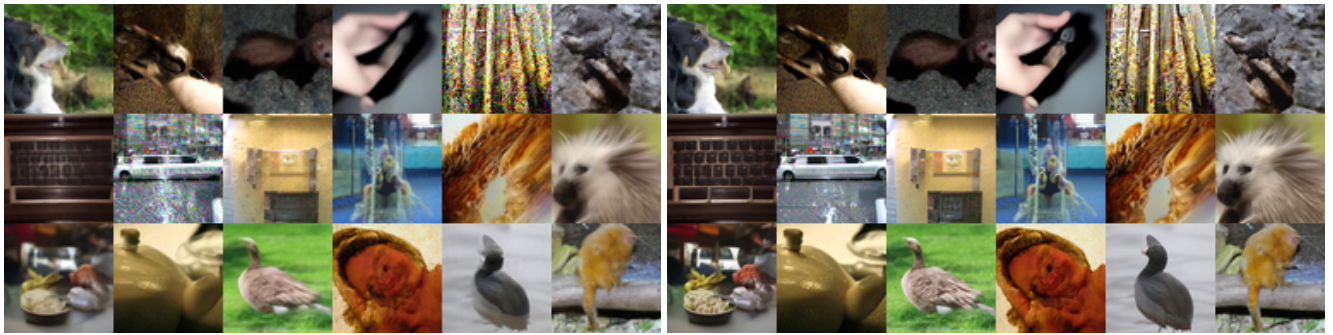
(d) iPNDM + PAS, NFE = 10, FID = 4.28

Figure 12. Random samples by iPNDM [21, 47] with and without the proposed PAS on FFHQ 64×64 [12].



(a) DDIM, NFE = 6, FID = 34.03

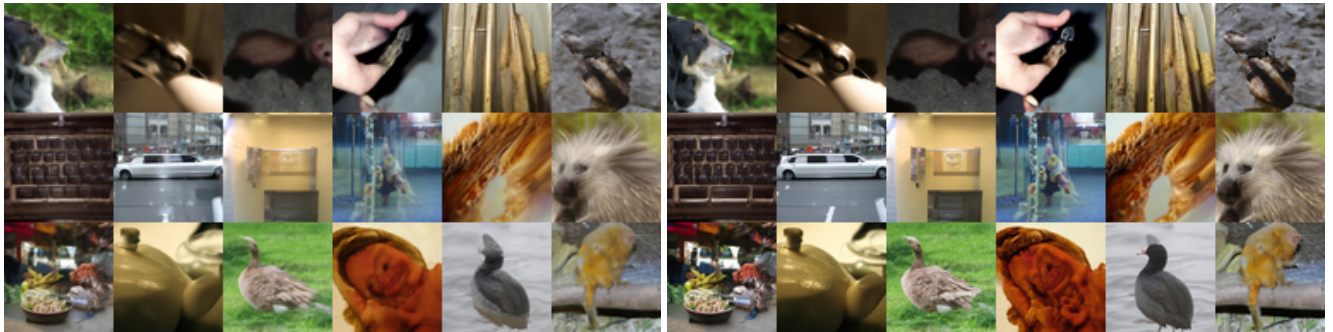
(b) DDIM, NFE = 10, FID = 16.72



(c) DDIM + PAS, NFE = 6, FID = 26.21

(d) DDIM + PAS, NFE = 10, FID = 9.13

Figure 13. Random samples by DDIM [36] with and without the proposed PAS on ImageNet 64×64 [6].



(a) iPNDM, NFE = 6, FID = 13.48

(b) iPNDM, NFE = 10, FID = 5.64



(c) iPNDM + PAS, NFE = 6, FID = 12.89

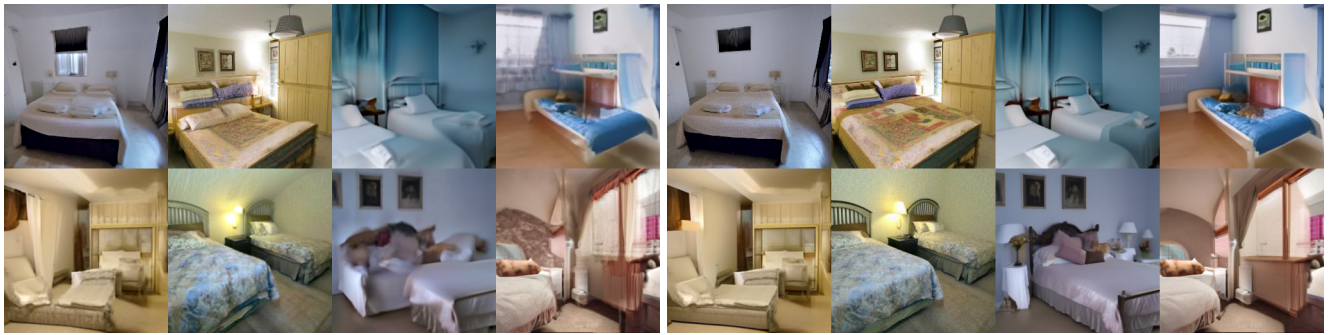
(d) iPNDM + PAS, NFE = 10, FID = 5.32

Figure 14. Random samples by iPNDM [21, 47] with and without the proposed PAS on ImageNet 64×64 [6].



(a) DDIM, NFE = 6, FID = 25.25

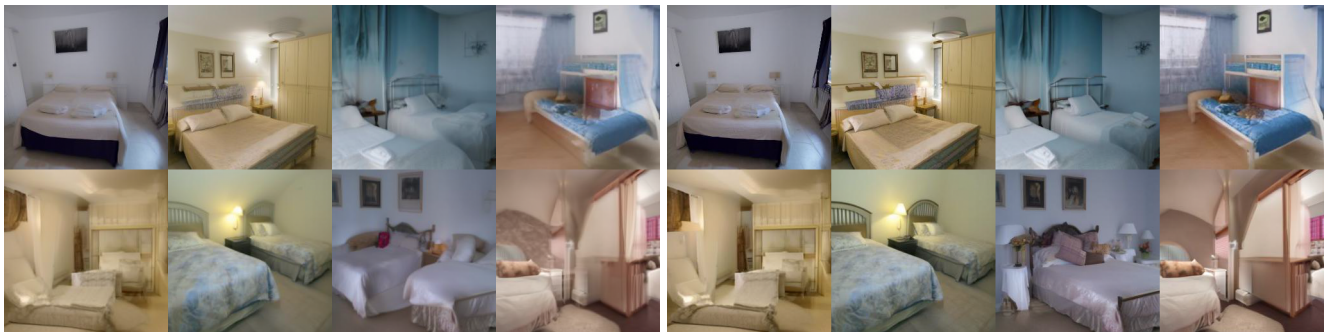
(b) DDIM, NFE = 10, FID = 11.42



(c) DDIM + PAS, NFE = 6, FID = 13.31

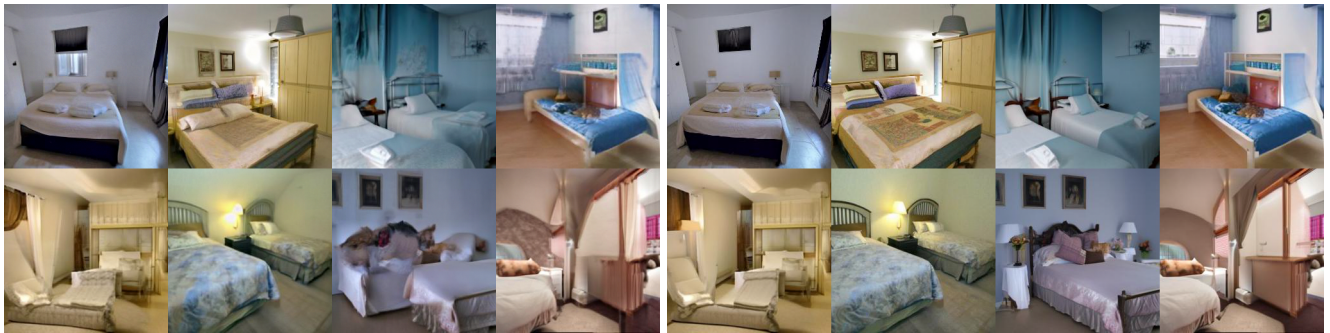
(d) DDIM + PAS, NFE = 10, FID = 6.23

Figure 15. Random samples by DDIM [36] with and without the proposed PAS on LSUN Bedroom 256×256 [45].



(a) iPNDM, NFE = 6, FID = 12.90

(b) iPNDM, NFE = 10, FID = 6.17



(c) iPNDM + PAS, NFE = 6, FID = 10.24

(d) iPNDM + PAS, NFE = 10, FID = 5.14

Figure 16. Random samples by iPNDM [21, 47] with and without the proposed PAS on LSUN Bedroom 256×256 [45].